ELSEVIER

Surface Science 376 (1997) 267–278

surface science

Strain relief during metal-on-metal electrodeposition: a scanning tunneling microscopy study of copper growth on Pt(100)

A.M. Bittner*, J. Wintterlin, G. Ertl

Fritz-Haber-Institut der Max-Planck-Gesellschaft, Faradayweg 4–6, D-14195 Berlin, Germany

Received 8 August 1996; accepted for publication 2 December 1996

Abstract

The galvanic deposition of copper on Pt(100)-(1 × 1) was studied in sulfate electrolyte by means of time-resolved in situ STM and voltammetry. Surprisingly, copper grows layer-by-layer in the absence of strongly adsorbing additives. This behavior persists beyond the deposition of two layers and is thus different from that found in analogous vacuum studies. After deposition of 5 to 10 layers, the deposit relaxes to the copper bulk structure. Due to the Cu–Pt misfit and the geometry of the Pt substrate, this results in a square-shaped moiré pattern. For thick layers, the growth proceeds in the usual way, i.e. via three-dimensional clusters.

Keywords: Copper; Epitaxy; Metal–electrolyte interfaces; Platinum; Scanning tunneling microscopy; Single crystal surfaces; Surface relaxation and reconstruction

1. Introduction

The classical Van der Merwe model [1,2] predicts that metal-on-metal heteroepitaxy is at first pseudomorphic, where the lattice misfit between the overgrowth and the substrate leads to elastic stress. After a critical thickness is reached dislocations are formed, which finally, at large thicknesses, completely accomodate the misfit. There are, however, numerous effects that deviate from this picture. Mostly by STM studies [3] it was found, e.g. that the misfit is not necessarily relieved in narrow dislocations and an almost pseudomorphic packing in between, but in a continuous contraction or expansion of the entire film. This can happen in several steps, at first only in one direction [4] resulting in similar structures as the Au(111) reconstruction, and only in a second step leading to a uniform contraction or expansion [4]. The overgrowth could then still be epitaxially aligned, causing a moiré pattern with a definite period (see e.g. Refs. [4,5]). It is also a known effect [6] that the strain can lead to formation of different bulk phases of the overgrowth. This was also observed by STM, where for Cu deposition on Pd(100) a bct (body centered tetragonal) Cu phase was detected [7]. For Cu on Ni(100) [8] dislocations have been detected, but their structure was significantly different from the edge dislocations assumed in the older models.

All of these observations are for molecular beam epitaxy (MBE) grown films in an ultra high vacuum (UHV) environment. For deposition of metals from electrolyte solutions such effects have

* Corresponding author. Present address: Institut de Physique Expérimentale (IPE), DP-EPFL, PHB-Ecublens, (H-1015 Lausanne, Switzerland. Fax: +41 21 6933604.

0039-6028/97/$17.00
PII S0039-6028(96)01395-7

not yet been reported in the literature. For electrodeposition of Pb on both Ag(111) and (100) a hexagonal moiré structure was found [9], but this appeared already in the first – underpotential deposition (UPD) – layer, apparently caused by the large diameter of the Pb atoms. Otherwise the UPD layers form mostly (1×1) or other simple structures directly after which 3D cluster growth sets in. This is the case, e.g. in the standard system Cu on Au surfaces [10,11]. (Pseudo-)layer-by-layer growth – where each new layer starts growing only after the topmost layer is (almost) completed – is a rare phenomenon, usually only found for small lattice mismatches, e.g. for Ag/Au(*hkl*) [12,13] and Ag/Pt(111) [14]. Reasons for the absence of the complex effects observed in UHV may be experimental problems, e.g. that the terraces on the usually obtained 3D islands are too small to detect similar effects by STM. A more interesting difference is the presence of the electrolyte which may change the surface energy of the deposit and hence the growth mode. For example, a known effect of coadsorbed anions is the frequent difference of the structure of the UPD layer compared to the monolayer prepared in UHV. Such effects of foreign compounds in the electrolyte can be used intentionally to control the film morphology by additives which act as surfactants [15] ("brighteners" in technical terms since they cause shiny surfaces). In this case one cannot expect to detect atomic scale dislocations since the surfactant will make up the topmost layer and it will strongly influence the film structure. During the preparation of this report we learned that Kolb et al. have recently found that Cu electrodeposited on Au(100) grows in a layer-by-layer fashion and that the Cu relaxes if the deposit is thicker than 10 layers [16].

In this study Cu was electrodeposited on a Pt(100) surface and the film structure followed by in situ electrochemical STM. The film thickness ranged from the UPD layer to 3D clusters where in the intermediate regime of pseudomorphic growth and relaxation similar effects as in UHV were observed. The (100) lattice constants of Pt and Cu are 0.277 and 0.255 nm, respectively; hence a pseudomorphic Cu film is under tensile strain. Since in our study the sample was flame annealed and quenched in water without potential control, the deposition takes place on the unreconstructed Pt substrate which was confirmed by the STM topographs. The hexagonal reconstruction of Pt(100) has been shown to be preserved in contact with the electrolyte only when the sample, after preparation in UHV, was emersed at negative potentials, but was lifted irreversibly at any other conditions [17]. UHV studies of Cu deposition on Pt(100), using LEED (low energy electron diffraction) and other techniques, have shown that the first layer grows pseudomorphically and relaxes to bulk Cu in the second layer [18]. Oxygen can act as a surfactant as has been shown for Cu/Pt(111) [19]. Bulk deposition of Cu on Pt(100) from electrolyte solutions has been studied before by a microscopic method, atomic force microscopy (AFM), only on a larger scale [20,21]. The use of Cu^{2+} concentrations of up to 250 mM and large overpotentials (up to 620 mV, corresponding to $-300\ mV_{SHE}$ (standard hydrogen electrode)) resulted in large current densities (up to $-0.3\ A\ cm^{-2}$) and 3D cluster growth on which no atomic details could be detected. For a better control of the film thickness in the present study STM images were taken at intermediate overpotentials (up to 430 mV in 10 mM Cu^{2+}, corresponding to $-150\ mV_{SHE}$) and low current densities (up to $-140\ \mu A\ cm^{-2}$).

2. Experimental

We employed a homebuilt STM described in Ref. [22] and a homebuilt potentiostat which can be switched to the galvanostatic mode. STM tips were made from iridium (99.9%, Goodfellow) by grinding a 0.25 mm wire to a fine apex. The tips were covered with Apiezon wax W on a length of ca. 4 mm except for the apex, thereby minimizing faradayic currents. The STM electrochemical cell was made of PCTFE ("kel-f"). A platinum wire served as a quasi-reference electrode. The counter electrode was a platinum wire; it was diffusionally shielded from the working electrode by placing the wire in a cylindrical opening that was connected to the main electrolyte compartment by means of a long and thin bore-hole. A layer of 2 to 3 mm of electrolyte covered the crystal.

The working electrode, a platinum crystal, was cut from a single crystal rod and mechanically and electrochemically polished [23]. In order to facilitate handling of the crystal the back side was welded to a platinum wire. Before an experiment the platinum crystal was annealed to yellow heat (ca. 1500 K) in a gas flame for several minutes, cooled to dark red heat (ca. 1000 K) in air and immediately quenched in triply distilled water, thereby protecting it with a drop of water. The crystal was then transferred to the STM electrochemical cell. After contacting the potentiostat, a glass bell covering the STM and the cell was closed and purged with nitrogen (5.0, Linde). Thereby the solution was de-aerated during subsequent potential scans. These could be run either between or during STM scans. Electrochemical potentials were measured with a platinum quasi-reference electrode (stability better than ± 10 mV) and – taking the potential of copper dissolution as a reference point – are quoted relative to the standard hydrogen electrode (SHE). All STM pictures were recorded in the constant current mode and are mainly presented as grayscale images (white designates the highest points, black the lowest). All of the images shown are unfiltered data.

Glass instruments (pipettes and storage flasks) were cleaned with chromosulfuric acid (Merck) and rinsed twice with boiling triply distilled water. Kel-f and teflon parts were cleaned in a mixture (ca. 5:1) of 96% H_2SO_4 (p.a., Merck) and 30% H_2O_2 (p.a., Merck) and rinsed with triply distilled water. Electrolytes were prepared from 96% H_2SO_4 (Suprapur, Merck), $CuSO_4$ (99.999%, Aldrich) and triply distilled water.

3. Results

Fig. 1 shows cyclic voltammograms of Pt(100) in $CuSO_4/H_2SO_4$ which were recorded in the STM

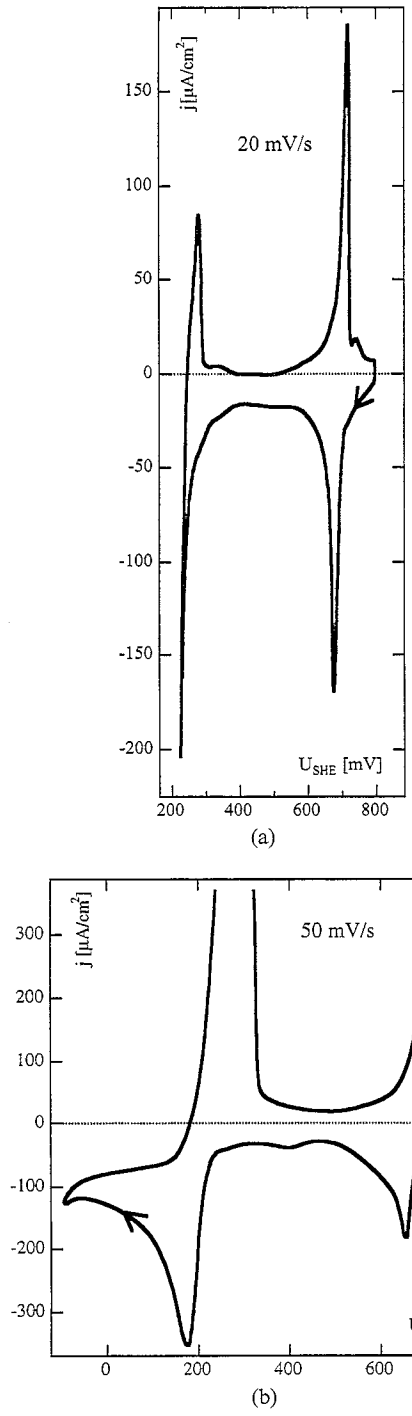

Fig. 1. (a) Cyclic voltammogram (20 mV s^{-1}) showing the deposition and stripping of a copper monolayer on flame-annealed and water-quenched Pt(100) in 10 mM $CuSO_4$ + 50 mM H_2SO_4. Recorded in the STM cell. (b) As in (a), but recorded in 1 mM $CuSO_4$ + 50 mM H_2SO_4, at the higher scan rate of 50 mV s^{-1} and to a potential below the onset of bulk deposition (250 mV_{SHE}).

electrochemical cell. Curve (a) was recorded at a scan speed of 20 mV s^{-1} in 10 mM Cu^{2+}, curve (b) at 50 mV s^{-1} to a more negative potential in 1 mM Cu^{2+}. The peaks at around 700 mV_{SHE} are caused by Cu UPD and stripping of the UPD layer; in contrast to the findings of earlier studies [24–28] the anodic and the cathodic peak are both similarly sharp as recently reported by other authors [29,30]. The UPD is somewhat sluggish, following from the fact that slightly faster potential scans shift the peak to more negative potentials and broaden it. The charge evaluated from the UPD peak amounts to about 400 $\mu C\,cm^{-2}$, equivalent to one monolayer (ML) of Cu atoms from which it is reasonable to assume that the UPD leads to a (1×1) layer of Cu atoms [27,28,30]. The features at more negative potentials are caused by Cu bulk deposition and dissolution, where the bulk deposition starts at the respective Cu/Cu^{2+} equilibrium potentials, e.g. at 250 mV_{SHE} for curve (b). It is seen that the voltammetric behavior depends critically on the potential scan speed. A cathodic sweep exhibited a current minimum (at ca. 170 mV_{SHE} in Fig. 1b). This reflects fast depletion of Cu^{2+} in the area in front of the surface resulting from the fact that the solution can not be stirred in the electrochemical STM cell so that a diffusion profile builds up.

A problem for STM experiments during bulk deposition is that also a lateral diffusion profile evolves. This is caused by the large tip radius which is probably in the 1 μm range, i.e. of the same order as the maximum scan range. Hence, there is only a small volume of electrolyte in front of the area under investigation into which diffusion is partially shielded by the tip, causing quick depletion of Cu^{2+} ions. By this effect less Cu is deposited at the area under the tip than at outside regions, and the thickness of the deposit monitored by STM could not be correlated with the charge from the cyclic voltammogram. Furthermore, observation of the film during growth was mostly possible only for relatively large Cu^{2+} concentrations of typically 10 mM which, however, sometimes led to an uncontrolled growth of large 3D islands into the STM image from areas outside. A better control of the film thickness was achieved by a reverse procedure: After deposition of a greater amount of Cu, with the tip pulled back (by >0.5 mm) the sample was disconnected by which the Cu/Cu^{2+} equilibrium potential established as open circuit potential. Small amounts of dissolved O_2 then caused dissolution[1] of the Cu which was followed by the STM and could be stopped at an intermediate thickness by again applying a more negative potential (about 100 mV_{SHE}). Because of the shielding effect this did not lead to renewed growth at the scan area. This procedure could be repeated until all Cu dissolved. After complete stripping the original structure of Pt(100) was always found. Hence alloy formation as in Cu UPD on Au(110) in the presence of Cl^- [31] can be excluded. Alloying between Cu and Pt(100) commences only at $T>550$ K in UHV [18,19].

In favorable cases – probably when by chance a mesoscopically sharper tip was used – it was possible to observe the growth of thicker deposits in situ. The series of STM topographs shown in Fig. 2 were recorded during deposition from a 1 mM Cu^{2+} solution. Each image took about 50 s, the slow scanning direction is indicated by arrows. Fig. 2a, taken about 1 min after polarisation at 120 mV_{SHE} (i.e. negative of the bulk deposition, see Fig. 1), shows roughly parallel diagonal terraces which, at the lower half of the image, are covered with many small dots. These probably represent Cu nuclei (height ca. 0.2 nm, diameter 1 to 1.5 nm, density 0.20 to 0.25 nm^{-2}) which have formed at defects of the Pt(100) substrate. Images of the clean Pt surface show many small hillocks (height 0.05 to 0.1 nm, diameter 1 to 2 nm, density 0.1 to 0.2 nm^{-2}). Their exact diameter is difficult to measure since they do not possess sharp step boundaries. They are immobile, do not depend on potential and are still present after Cu bulk deposition and dissolution. It is not quite clear so far if they represent contaminant atoms – this appears less likely because cyclic voltammograms of the freshly prepared Pt(100) in H_2SO_4 indicate a very clean surface – or Pt atoms, possibly resulting from the lifting of the "hex" reconstruction during

[1] Even in usual electrochemical cells where nitrogen is bubbled though the electrolyte, traces of O_2 can cause dissolution of copper.

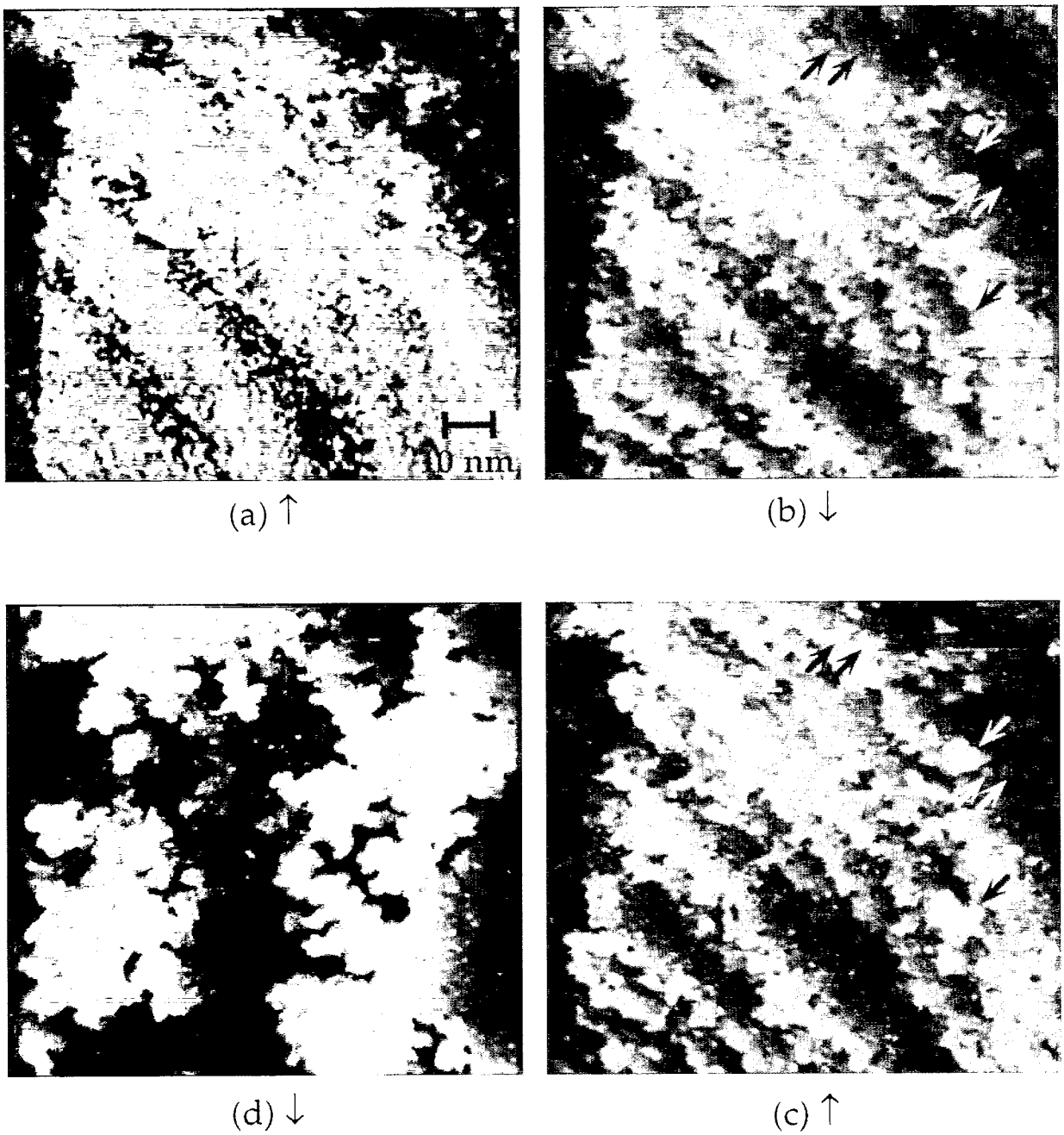

Fig. 2. (a), (b), (c) Consecutive STM images (each 50 s) showing the deposition of several layers of copper. The arrows outside the images indicate the slow scan direction; the arrows in (b) and (c) point out areas where fresh copper islands grow. 109 nm × 101 nm, 120 mV_{SHE}, $-20\ \mu A\ cm^{-2}$, 1 mM $CuSO_4$ + 50 mM H_2SO_4. Tip potential 130 mV_{SHE}, tunneling current 4 nA. (d) The same area 100 s later.

cool down of the flame annealed crystal. In any event they offer many nucleation sites on the flat terraces. The Cu UPD layer which should be present at the applied potential (see Fig. 1) was not resolved. At about the center of Fig. 2a growth of Cu islands sets in. Different from Cu deposition on Au(100) [11], steps do not play any role for the nucleation. In Fig. 2b islands have become larger, covering the terraces almost completely. At the locations marked by arrows in Fig. 2b and Fig. 2c, islands of the next Cu layer have started to grow, which also coalesce. Fig. 2d shows the same area at a later stage (two images between (c) and (d) are left out), in which the Cu islands have grown to appreciable sizes and do not show any correlation with the original terraces of the Pt substrate. The shape of the islands is irregular, steps do not run along the main crystallographic directions. In some cases, especially at very negative potentials ($-150\ mV_{SHE}$), steps appeared frizzy which may be connected with the high mobility of Cu atoms (see Ref. [32]).

The coalescing islands leave relatively large holes upon percolation which become, however, filled by additional Cu. The resulting morphology is smooth, and even the point defects at the substrate do not cause inhomogeneities. The step height of about 0.18 nm is within experimental errors identical to that of the Pt(100) substrate. Accordingly, the larger islands which extend over several substrate terraces – e.g. the one at the bottom right corner – do not show dislocations at the positions of the underlying Pt steps. These would be seen as small steps with a height identical to the difference between the Pt layer and Cu film layer spacings which is apparently below the resolution limit.

Atomically resolved images of the Cu islands reveal a square lattice with a unit cell of $0.28\ nm \times 0.28\ nm$ (Fig. 3). This is identical to the lattice constant of the Pt(100) substrate of 0.277 nm and hence in agreement with a pseudomorphic growth. The dark spots in the image are probably Cu vacancies. We conclude that several layers of Cu grow pseudomorphically, in a pseudo-layer-by-layer fashion.

Fig. 4 shows data in which the deposition of a thicker Cu film could be monitored in situ. The three frames were recorded successively on the same area (note the bright defect at the upper edge), with the slow scanning direction again marked by arrows. The starting situation at $155\ mV_{SHE}$ (Fig. 4a and top of Fig. 4b) was reached by deposition followed by almost complete dissolution of Cu. The image is, similarly as in Fig. 2a, characterized by bands of Pt terraces already covered with small islands of Cu. At the top of the second topograph the potential was suddenly lowered to $-145\ mV_{SHE}$ which is very far in the bulk deposition regime (see the cyclic voltammogram for a 1 mM solution in Fig. 1b). As seen at the top of the image, this led to the sudden formation of a thicker film. In the following image (c) the surface is completely covered with Cu. At the upper half of the image, where the film is less thick (the Pt steps as seen in (a) descend from top to bottom), the islands are flat and have similar shapes as those in Fig. 2. In this part the deposit has therefore grown pseudomorphically, as before. At the lower half and the right part of the image, however, the islands are corrugated. Since the resulting Cu terraces are, on average, wider than those of the original Pt surface, the overgrowth must be thicker at the lower half and the right part of the image, and the corrugated phase must hence be connected with a greater thickness. This follows also from the fact that, on the wider Cu terraces, the structure changes from flat to corrugated as one moves from the top to the bottom edge of the terrace. From the distance the tip pulled back at the top of Fig. 4b, where

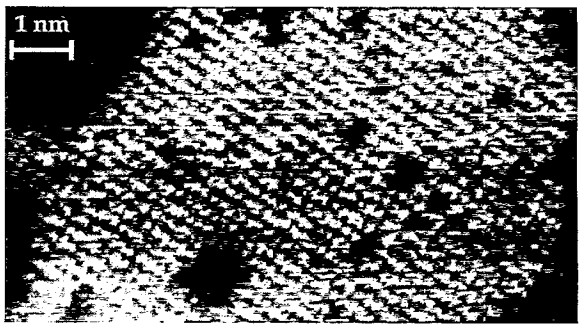

Fig. 3. Atomically resolved surface (9.7 nm × 5.3 nm) of copper layers on Pt(100) in 1 mM $CuSO_4$ + 50 mM H_2SO_4 at $110\ mV_{SHE}$ ($-20\ \mu A\ cm^{-2}$). Tip potential $320\ mV_{SHE}$, tunneling current 10.5 nA.

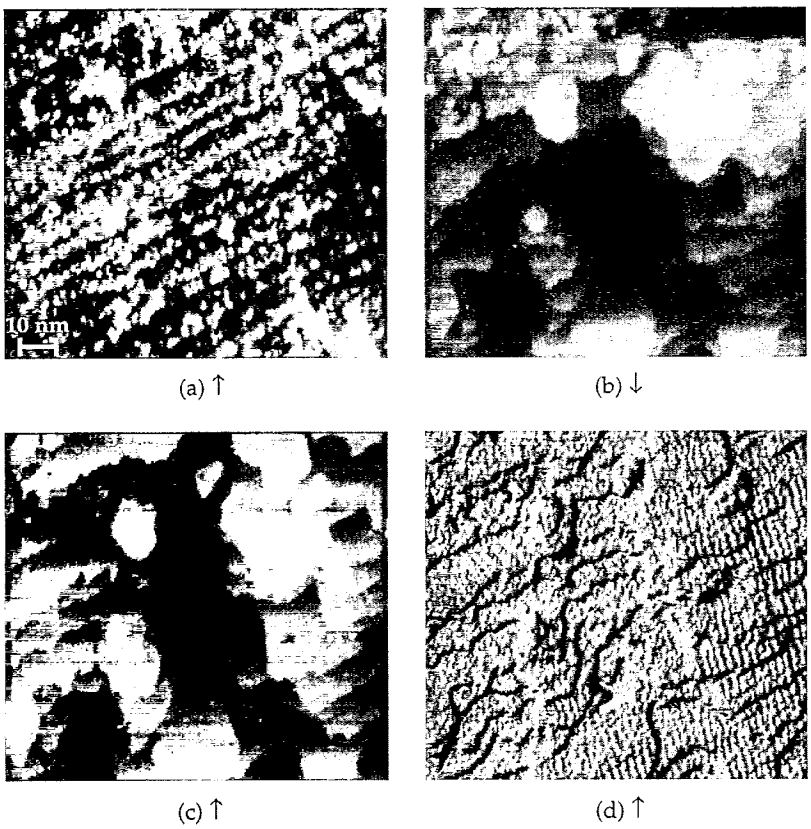

Fig. 4. Cu/Pt(100) in 10 mM $CuSO_4$ + 50 mM H_2SO_4 (107 nm × 101 nm, tip 330 mV_{SHE}, 10.5 nA). The arrows outside the images indicate the slow scan direction. (a) 155 mV_{SHE} (ca. 0 $\mu A\,cm^{-2}$); after deposition and almost complete dissolution of copper some islands are left over. In the upper part of the following image (b) the potential is suddenly lowered to −145 mV_{SHE} (−110 $\mu A\,cm^{-2}$) resulting in the deposition of about 8 extra copper layers. A square-shaped corrugation on the copper terraces becomes visible here and in the following image (c). Side illumination (d) enhances the contrast (here shown for image (c)). The upper left part of (b), (c) and (d) is covered by a pseudomorphic Cu layer featuring smooth terraces and small Cu islands as in Fig. 2.

the potential was changed, the thickness at which the structure transition from the pseudomorphic to the corrugated phase occurs is estimated to be between 5 and 10 ML. This thickness is much bigger than a possible change in the tip–sample distance caused by the the lowering of the potential alone. In the absence of metal ions such a change of the potential results at most in vertical jumps of about 1 ML height.

The corrugated phase is further characterized by Figs. 5 and 6. The topograph displayed in Fig. 5 shows that it is possible to prepare a Cu film that consists entirely of the corrugated phase. It is seen that the morphology is different from that of the thinner, pseudomorphic film. In contrast to the irregular islands with irregularly shaped rounded edges (see Fig. 2), the corrugated phase features – albeit also with rounded edges – an almost rectangular terrace shape. Fig. 6 displays the Cu lattice of the corrugated phase with atomic resolution. It is seen that the corrugation pattern and the atomic lattice are aligned. The lateral period of the corrugation amounts to 3.3 nm (this value is somewhat variable, in some parts of Fig. 6 it is smaller), the corrugation amplitude to 0.05 nm.

A model that explains these features is shown in Fig. 7. It is formed by placing a Cu(100) layer, with the bulk lattice constant of 0.255 nm, on top

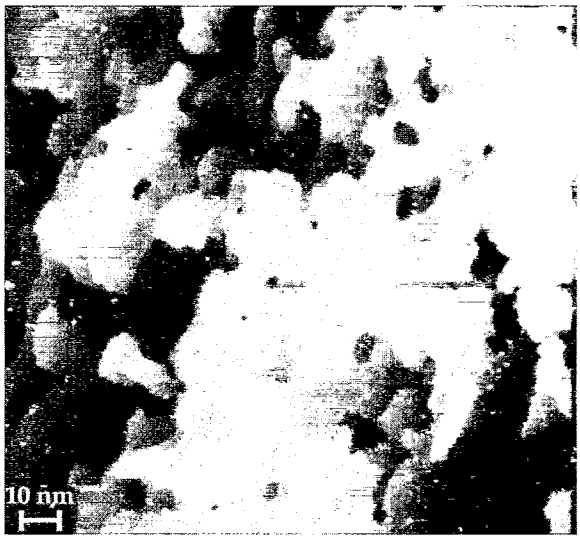

Fig. 5. STM image (152 nm × 142 nm) of a completely relaxed Cu surface. All of the almost rectangularly shaped terraces are covered by the corrugated copper phase. 1 mM $CuSO_4$ + 50 mM H_2SO_4, −80 mV_{SHE}, −110 $\mu A\,cm^{-2}$ (tip 320 mV_{SHE}, 1.5 nA).

Fig. 6. Surface (14.2 nm × 12.4 nm) of the corrugated copper phase on Pt(100) in 1 mM $CuSO_4$ + 50 mM H_2SO_4 at −80 mV_{SHE} (−53 $\mu A\,cm^{-2}$). The image reveals a slightly distorted atomic moiré pattern that is aligned to the directions of steps as seen for the square-shaped hole in the lower right part. Tip potential 320 mV_{SHE}, tunneling current 27 nA.

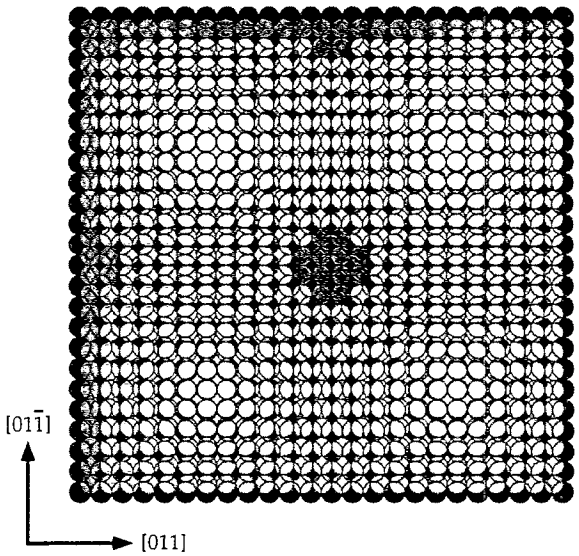

Fig. 7. Model of an ideal Cu(100) plane on a Pt(100)-(1 × 1)-substrate (dark circles mark Pt atoms). The Cu–Pt misfit produces a square-shaped moiré pattern with a period of 3.3 nm almost matching the patterns in Figs. 4–6.

of the ideal Pt(100) surface (period 0.277 nm), with the crystallographic directions aligned. (For clarity only one Cu layer is shown; the actual deposit consists of a slab of several layers.) This creates a square-shaped Moiré pattern, the period of which is given by the Cu–Pt misfit. 13 Cu lattice spacings correspond to about 12 Pt spacings, leading to a wavelength of 3.3 nm, which is consistent with the experimental value. The corrugation detected by STM is caused by the different positions of the atoms in the overlayer which shift from hollow (darker spheres in the model) to top sites (white spheres). In a hard sphere model this creates a corrugation of 0.075 nm, in agreement with experiment. The model can also explain the characteristic morphology which is visible in the atomically resolved image of Fig. 6: The dark rectangle represents a monolayer deep hole, the size of which is roughly identical to a unit cell of the moiré pattern, and the steps run along the close packed directions. This can be understood from the fact that the valleys of the moiré phase are energetically favored as a result of the more favorable hollow and bridge positions of the atoms in these areas. It is concluded that at between 5

and 10 ML of Cu the deposit relaxes to the lattice constant of bulk copper. The film remains, however, epitaxially aligned, leading to a moiré phase with a definite structure.

An additional structure, observed for the thicker films, is shown in Fig. 8. The surface had been prepared after the "reverse" technique described above, where the dissolution was stopped at a thicker Cu film. The image displays the pseudomorphic structure in the left part, the Moiré phase in the center, and a third structure at the bottom. The latter is characterized by a pattern of 2 to 3 nm wide stripes which run into two perpendicular directions. From the orientation of the moiré phase, these correspond roughly to the [011] and [01$\bar{1}$] directions. The height modulation between the brighter and darker stripes amounts to about 0.1 nm. After recording the image, most of the Cu was dissolved by an additional potential sweep which led to a terraced surface, with steps running about into the same direction as in Fig. 4, also descending from top to bottom. Since the deposit in Fig. 8 is, except for the left part, approximately on the same height level, this means that the film thickness increases from top to bottom. The additional structure corresponds hence to a yet thicker film than the moiré phase. We do not present a structure model for this phase, but it appears that dislocations are involved.

Finally, after deposition of still larger amounts of Cu (onto areas with similar Pt step geometry as in Figs. 2a and 4a), images like that shown in Fig. 9 were obtained in which Cu is seen to form extended 3D islands. (Such surfaces represented the starting situation of the dissolution technique that was mostly employed.) They still show horizontal terraces, indicating a definite orientation with respect to the substrate, which is supported by occasional resolution of a (1×1) lattice on top of the islands.

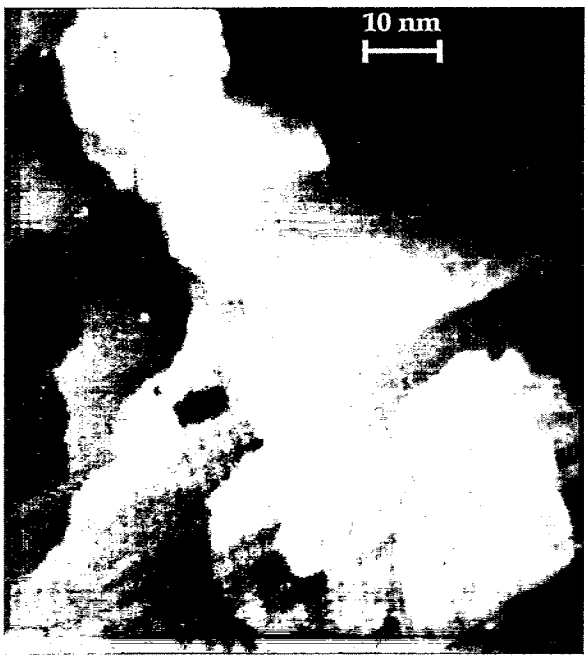

Fig. 8. STM image (78.6 nm × 89.3 nm) of the Cu/Pt(100) moiré phase in 10 mM $CuSO_4$ + 50 mM H_2SO_4 at −145 mV_{SHE} (−141 $\mu A\,cm^{-2}$). In the lower part stripes show up. They run parallel to the steps from the left lower corner to the right part of the picture. Tip potential 325 mV_{SHE}, tunneling current 10.5 nA.

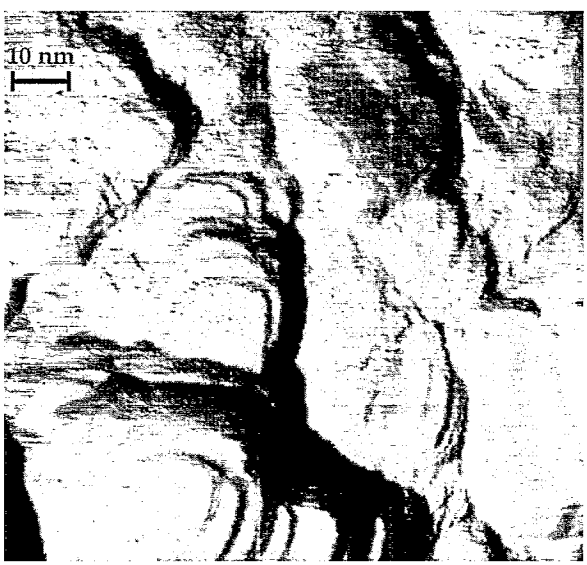

Fig. 9. STM image (105 nm × 101 nm) of a very thick 3D-copper cluster deposit grown from 1 mM $CuSO_4$ + 50 mM H_2SO_4 on Pt(100). The potential was swept to 140 mV_{SHE} which resulted in ca. −85 $\mu A\,cm^{-2}$. Tip potential 930 mV_{SHE}, tunneling current 10.5 nA.

4. Discussion

The STM data show that, after the UPD of a single layer, Cu electrodeposition on Pt(100) follows roughly a scenario that is found for many systems under vacuum conditions: pseudomorphic growth, relaxation to the bulk lattice and 3D cluster growth. This scenario has so far only partially been detected under electrolyte. However, there are also features which are different from systems studied in vacuum. The pseudomorphic growth continues up to 5 to 10 ML (Fig. 10), which is quite thick considering the large misfit of 8.6% between Cu and Pt. With this value it is estimated, based on the classical Van der Merwe model, that the stress building up in the overgrowth should create dislocations already for a film thicker than 1 ML [1]. This is in agreement with results of an experimental study on Cu/Pt(100) in vacuum [18] in which LEED spots of the bulk Cu lattice were observed for films thicker than 1 ML. It does not appear very likely that different kinetic restrictions in vacuum and under electrolyte are responsible for this difference. The surface mobility of Cu atoms on top of a growing Cu film is generally high enough to form sizeable islands [4] which is the case also under electrolyte as revealed by the present data. Anions usually rather increase the surface mobility of metal atoms [33,34]. On the other hand, it could be argued that the formation of the Moiré phase, given it involves all or most of the Cu layers as shown in Fig. 10, requires a structure rearrangement of the entire film and might therefore be connected with a larger kinetic barrier. In the in situ experiments the structure transformation was, however, so fast that it could not be resolved (in time) by STM. We note that the electrodeposition of Cu on Au(100) [16] appears to follow a similar scenario.

We propose therefore that the different growth mode is a thermodynamic effect, caused by a changed surface stress in the presence of the electrolyte. Employing STM to measure the deformation of a sample in contact with electrolyte, Haiss and Sass [35] determined changes of the surface stress during electrodeposition of Cu on a Au(111) surface from $CuSO_4/H_2SO_4$. It was found that a Cu monolayer, formed by UPD, causes compressive stress rather than the tensile stress expected from the smaller lattice constant of Cu. This may be attributed to the simultaneous coadsorption of sulfate which, as a charged particle, leads to compressive stress. Such an effect of adsorbed sulfate has to be considered also in the potential range of bulk deposition, for which radioactive marker experiments [36] revealed the presence of adsorbed sulfate. For thicker films the relative contribution of the Cu increases, of course, so that at about 5 ML the net stress becomes tensile [37]. Different from the situation in UHV, the electrodeposited pseudomorphic Cu film on Pt(100) may hence be stabilized up to greater thicknesses by counteracting stresses of the Cu film and the adsorbed sulfate ions.

At about 5 to 10 ML the tensile stress apparently exceeds a critical value, and the film relaxes to the lattice constant of bulk Cu. It can not be directly derived from the STM topographs whether this affects the entire film (possibly except for the first layer), as assumed in the model displayed in Fig. 10, or only one or several layers at the top.

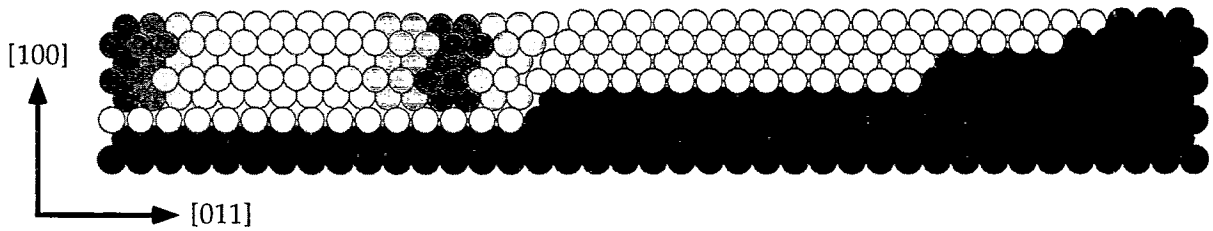

Fig. 10. Side view model of Cu/Pt(100)-(1 × 1) (dark circles mark Pt atoms). Up to ca. 5 layers copper grows pseudomorphically as shown in the right part. Thicker layers relax to the copper bulk phase (except probably for the first layer), and the Cu–Pt misfit causes a corrugation (white-grey circles). A top view is displayed in Fig. 7.

However, the fact that the transformation occurs only after a certain thickness is reached indicates that the transformation is determined by the energy balance between the stress of the pseudomorphic film and the energy contained in the interface between the relaxed film and the substrate. Since the latter should be largely independent of the thickness it is energetically more favorable when the entire film relaxes once the stress is large enough. It can, however, not be ruled out that the bottom Cu layer, which feels a different chemical surrounding than the rest of the film, is still pseudomorphic. Moiré structures in metal-on-metal epitaxy – which often feature slightly variable lattice spacings – have been observed in many cases on hexagonal or quasi-hexagonal substrates, e.g. for Cu/Ru(0001) [4], Cu/Pt(111) [38–40] and Fe/W(110) [5]. However, for a quadratic substrate a moiré phase was, to our knowledge, not found before (except for the hexagonal arrangement of the above-mentioned Pb UPD on Ag(100) [9]). For Cu/Pd(100) (in vacuum) [7], for which the misfit of 7.8% is very similar to Cu/Pt(100), the first layer (at 300 K) grows pseudomorphically; for thicker films a bct (body centered tetragonal) Cu structure is formed which has the same lateral lattice spacing as the Pd, but a strongly reduced layer distance (0.155 nm compared to 0.195 nm for the Pd). Bct Cu was detected in the STM images by this difference which shows up as small steps of 0.04 nm height. Steps of 0.04 nm would also be expected for Cu/Pt(100), but were not detected; hence the formation of a bct phase of Cu appears unlikely. This may be explained by the fact that the relaxation happens at a relatively large thickness for which the bct phase may no longer be stable. Another sytem, Ni/Cu(100), for which the overgrowth is also under tensile stress, behaves differently, too [41]; it probably follows the classical dislocation scheme of Van der Merwe.

5. Summary

We have employed STM and voltammetry to follow the growth of a Cu deposit on Pt(100) from $CuSO_4/H_2SO_4$ solutions with time-resolution. We find that the Cu builds up via UPD, pseudomorphic growth of 5 to 10 ML in a (pseudo-)layer-by-layer fashion, relaxation to a moiré phase, and formation of 3D clusters of bulk Cu, with probably an additional relaxed phase in between. The relatively large thickness of the pseudomorphic film which is under tensile stress can be explained by the counteracting compressive stress caused by adsorbed sulfate ions. The square-shaped moiré phase is formed by overlaying a (100) oriented slab of bulk Cu onto the Pt substrate lattice, with aligned crystallographic directions; the periodicty is given by the Cu–Pt misfit. Thereby we have also shown that copper single crystals with (100) orientation can be grown by electrodeposition on a Pt(100) substrate without application of strongly adsorbing additives. This circumvents the usual ex situ preparation of Cu crystals that is mainly based on etching techniques (see Ref. [42]).

References

[1] J.H. van der Merwe and C.A.B. Ball, in: Materials Science Series: Epitaxial Growth Part B, Ed. J.W. Matthews (Academic Press, London, 1975) p. 493.
[2] W.A. Jesser and D. Kuhlmann-Wilsdorf, Phys. Stat. Solidi 19 (1967) 95.
[3] J. Wintterlin and R.J. Behm, in: Scanning Tunneling Microscopy I, Springer Series in Surface Science, Eds. H.-J. Güntherodt and R. Wiesendanger (Springer, Berlin, 1994) p. 38.
[4] C. Günther, J. Vrijmoeth, R.Q. Hwang and R.J. Behm, Phys. Rev. Lett. 74 (1995) 754.
[5] H. Bethge, D. Heuer, C. Jensen, K. Reshöft and U. Köhler, Surf. Sci. 331 (1995) 878.
[6] R. Bruinsma and A. Zangwill, J. Physique 47 (1986) 2055.
[7] E. Hahn, E. Kampshoff, N. Wälchli and K. Kern, Phys. Rev. Lett. 74 (1995) 1803.
[8] B. Müller, B. Fischer, L. Nedelmann, A. Fricke and K. Kern, Phys. Rev. Lett. 76 (1996) 2358.
[9] W. Obretenov, U. Schmidt, W.J. Lorenz, G. Staikov, E. Budevski, D. Carnal, U. Müller, H. Siegenthaler and E. Schmidt, J. Electrochem. Soc. 140 (1993) 692.
[10] R.J. Nichols, D.M. Kolb and R.J. Behm, J. Electroanal. Chem. 313 (1991) 109.
[11] N. Batina, T. Will and D.M. Kolb, Disc. Faraday Soc. 94 (1992) 93.
[12] E. Budevski, G. Staikov and W.J. Lorenz, Electrochemical Phase Formation and Growth (VCH, Weinheim, 1996).
[13] T. Hachiya and K. Itaya, Ultramicroscopy 42–44 (1992) 445.

[14] N. Kimizuka and K. Itaya, Disc. Faraday Soc. 94 (1992) 117.
[15] R.J. Nichols, W. Beckmann, H. Meyer, N. Batina and D.M. Kolb, J. Electroanal. Chem. 330 (1992) 381.
[16] D.M. Kolb (private communication); some preliminary results can be found in Ref. [12] p. 197.
[17] M.S. Zei, N. Batina and D.M. Kolb, Surf. Sci. 306 (1994) L519.
[18] J. Radnik, B.D. Wagner, K. Oster and K. Wandelt, Surf. Sci. 357–358 (1996) 943.
[19] K. Oster, M. Schmidt, M. Nohlen, J. Radnik and K. Wandelt, Phys. Stat. Sol. (B) 192 (1995) 441.
[20] R.M. Rynders and R.C. Alkire, J. Electrochem. Soc. 141 (1994) 1166.
[21] W.U. Schmidt and R.C. Alkire, J. Electrochem. Soc. 141 (1994) L85.
[22] A.M. Bittner, J. Wintterlin and G. Ertl, J. Electroanal. Chem. 388 (1995) 225.
[23] A.M. Bittner, J. Wintterlin, B. Beran and G. Ertl, Surf. Sci. 335 (1995) 291.
[24] D.M. Kolb, R. Kötz and K. Yamamoto, Surf. Sci. 87 (1979) 20.
[25] C.L. Scortichini and C.N. Reilley, J. Electroanal. Chem. 139 (1982) 233.
[26] D.P. Bhatt, T. Twomey, W. Plieth, R. Schumacher and H. Meyer, J. Electroanal. Chem. 322 (1992) 279.
[27] N.M. Markovic and P.N. Ross, Langmuir 9 (1993) 480.
[28] D. Aberdam, Y. Gauthier, R. Durand and R. Faure, Surf. Sci. 306 (1994) 114.
[29] H. Matsumoto, J. Inukai and M. Ito, J. Electroanal. Chem. 379 (1994) 223.
[30] M.S. Zei and G. Ertl, Ber. Bunsenges, Phys. Chem., submitted.
[31] F. Möller, O.M. Magnussen and R.J. Behm, Electrochim. Acta 40 (1995) 1259.
[32] M. Dietterle, T. Will and D.M. Kolb, Surf. Sci. 327 (1995) L495.
[33] I. Villegas and M.J. Weaver, J. Electroanal. Chem. 373 (1994) 245.
[34] D.M. Kolb, R.J. Nichols and R.J. Behm, in: Electrified Interfaces in Physics, Chemistry and Biology, Ed. R. Guidelli (Kluwer Academic Publishers, Dordrecht, 1992) p. 275.
[35] W. Haiss and J.K. Sass, J. Electroanal. Chem. 386 (1995) 267.
[36] P. Zelenay and A. Wieckowski, J. Electrochem. Soc. 139 (1992) 2552.
[37] W. Haiss (private communication).
[38] S. Gestermann, M. Nohlen, M. Schmidt and K. Wandelt, Verhandl. DPG (VI) 31 (1996) 1914 (O.39.7).
[39] M. Schmidt, Thesis, University of Bonn, Germany, (1995).
[40] R.C. Yeates and G.A. Somorjai, Surf. Sci. 134 (1983) 729.
[41] J.W. Matthews and J.L. Crawford, Thin Solid Films 5 (1970) 187.
[42] S. Härtinger and K. Doblhofer, J. Electroanal. Chem. 380 (1995) 185.